

# Bi-level Optimal Configuration of Energy Storage System in Distribution Network Using an Improved Grey Wolf Optimization Algorithm

Fengli Jiang, Kaiyuan Xue, Yunuo Wang, Zeyu Liu, Hang Zhang, Youwen Tian \*

**Abstract**—A bi-level optimization model for Battery Energy Storage Systems (BESS) was proposed, focusing on both economic efficiency and reliability. The model effectively alleviated the timing mismatch between new energy generation and load demands. The upper level solved the connection location and optimal capacity of the BESS with the objective of minimizing the average daily costs of the BESS. The lower level determined the daily operation strategy of the BESS by minimizing the vulnerability of the power grid, reducing peak load shavings, and enhancing the ability to suppress load fluctuations. An improved grey wolf optimization algorithm (IGWO) was employed to solve this model, and an analytic hierarchy process (AHP) method was used at the lower level to determine the weight coefficients of each objective. The model's effectiveness was investigated through simulations on the modified IEEE-33 bus system. The results demonstrated that the proposed bi-level optimization model for energy storage not only achieved optimal benefits but also improved load fluctuation and voltage quality.

**Index Terms**—Battery energy storage system; bi-level model; improved GWO algorithm; analytic hierarchy process

## I. INTRODUCTION

In recent years, as energy supplies have tightened, China has intensified efforts to clean its energy sources under the dual-carbon target [1]-[2]. Distributed Generations (DGs), primarily photovoltaics (PV) and wind turbines (WT), have developed rapidly due to their cleanliness and environmental friendliness. Due to the intermittent and uncertain nature of their output, the extensive integration of DGs into distribution networks may lead to voltage violations, changes in power flow distribution, and system losses increase, which

may adversely affect the safe, economical, and stable operation of the system [3]-[5]. Battery Energy Storage Systems (BESSs) have flexible power supply and storage capabilities, making them effectively alleviate the timing mismatch between new energy generation and load demands. In addition, they can reduce the abandoning of wind and solar power, fully leveraging the advantages of renewable energy sources [6]. The proper configuration of energy storage systems is particularly important in distribution systems with DGs. Excessive capacity and improper connection locations can have a direct impact on the high efficiency and economic functioning of the distribution networks, while insufficient capacity has a minimal effect on enhancing system operational efficiency [7]-[8]. Numerous scholars have conducted studies on the selection of sites and capacity determination of BESS. The reference [9] proposed a strategy to optimally allocate distributed ESS size by injecting P and Q into the distribution network through ESS, and a multi-objective energy storage siting and capacity optimization model was established to improve voltage quality and reduce power loss. A method in [10] was proposed for an optimal configuration of micropower sources and energy storage devices based on optimal expectations of power characteristics. This method aimed to minimize the average fluctuation rate of the total output power of micro-sources and micro-grid to effectively reduce the maximum adjustable power and available capacity of ESS. In the reference [11], a capacity optimization allocation method for BESS considering the primary frequency regulation rate characteristics was proposed to increase the frequency regulation capability and performance of the power system. However, the above models did not start from the economics of installing energy storage, which might lead to high installation and maintenance costs. The reference [12] constructed an active distribution network planning model with dynamic configuration of energy storage, and validated the model with four scenarios proposed in spring, summer, autumn and winter, which effectively improved the reliability of electricity consumption and operation economy. The reference [13] proposed an optimal planning scheme for grid integration of photovoltaics and energy storage, which effectively maintained the balance between economics and carbon emissions within the active distribution network. Bi-level optimization, as an effective method for solving energy storage system planning problems, has been widely applied in power systems. Table 1 shows the progress of research on the optimal allocation of energy storage using bi-level optimization over the year.

Manuscript received May 7, 2024; revised December 24, 2024.

Fengli Jiang is an associate professor of the College of Information and Electrical Engineering, Shenyang Agricultural University, Shenyang 110161, China (e-mail: fengli0308@163.com)

Kaiyuan Xue is a squad member of the State Grid Liaoning Electric Power Co., LTD Dalian Power Supply Company, Dalian 116001, China (e-mail: xueky122625@163.com)

Yunuo Wang is a postgraduate student of the College of Information and Electrical Engineering, Shenyang Agricultural University, Shenyang 110161, China (e-mail: 15524484178@163.com)

Zeyu Liu is a postgraduate student of the College of Information and Electrical Engineering, Shenyang Agricultural University, Shenyang 110161, China (e-mail: liuzy241125@163.com)

Hang Zhang is a postgraduate student of the College of Information and Electrical Engineering, Shenyang Agricultural University, Shenyang 110161, China (e-mail: 17542761506@163.com)

Youwen Tian is a professor of the College of Information and Electrical Engineering, Shenyang Agricultural University, Shenyang 110161, China (corresponding author to provide phone: 86- 13079231996; e-mail: youwen\_tian10@163.com)

TABLE I  
COMPARISON OF RELATED STUDIES

Upper level model objective function	Lower level model objective function	Optimization algorithm	Reference
Annual cost: equipment investment cost, operation and maintenance cost, power purchase cost from the power grid	Energy storage charging and discharging costs	IBPSO	14
Total cost of investment in distribution network operations: the total cost of distribution network operation investment, the input costs for energy storage construction	Voltage fluctuations; Load fluctuations	GA+IMOPSO	15
The total planning cost of the ESS in the distribution network: the investment and construction cost of energy storage, operation and maintenance cost, auxiliary equipment cost	The utilization rate of the energy storage battery; Indicator of daily voltage deviation; The network loss rate	PSO+NSGA-III	16
The present value of total cost: the current value of the investment cost, the present value of operating cost	Anti-burst capability index of distribution network	Mathematical method	17
The average daily costs of BESS: the daily investment cost, daily maintenance cost, daily charging and discharging cost and daily generation subsidy of the BESS	Grid vulnerability indicators; Peak load shaving; Suppression of fluctuations	IGWO	This paper

The reference [14] established a bi-level model for the joint operation of distributed power supply and energy storage in distribution networks, and improved the particle swarm algorithm by using chaotic optimization, which effectively improved the economy of operation and voltage distribution. Reference [15] presented an optimal allocation strategy for energy storage capacity in distribution network, which enhanced operational economy and mitigated voltage and load fluctuations. A bi-level optimization model for multi-point energy storage was established in reference [16] considering the service life of energy storage, which effectively reduced the planning cost and voltage fluctuation rate. The use of a variety of renewable energy sources and energy storage for distribution network planning guaranteed the economic operation of the distribution network and improved the reliability of a single emergency outage[17]. The above-mentioned references only considered one or a few of the indicators of economy or reliability in distribution network operation for the optimal configuration of BESS. However, in the optimization process, factors such as economy, safety, and reliability are often contradictory. Optimization based solely on a single-sided metric cannot meet the practical engineering requirements. Furthermore, the optimization configuration of BESS presents challenges such as multi-dimensionality, complex coupling relationships and huge computation. The reference [18] employed a multi-objective non-dominated sorting genetic algorithm to solve the multi-objective model of BESS. However, this algorithm exhibited strong randomness in its crossover and mutation operations. Similarly, as a mainstream algorithm, the Particle Swarm Optimization (PSO) algorithm was known for its fast convergence and simple structure, but it was prone to getting trapped in local optima [19].

To address the issues mentioned above, a bi-level optimization configuration model for BESS in this paper was established through the following four points: (1) A bi-level model was used for planning the configuration of BESS. The upper level model optimized the average daily cost of BESS, while the lower level model focused on optimizing the power grid's vulnerability index, peak load shaving, and the ability to stabilize load fluctuations. (2) The analytic hierarchy process method (AHP) was adopted to determine the weight coefficients of the objectives at the lower level optimization model. (3) An improved grey wolf optimization algorithm (IGWO) was proposed, which

iteratively solved the upper and lower level optimization models, avoiding issues such as getting trapped in local optima, common in traditional multi-objective algorithms. (4) The impact of BESS with different SOC limits and the number of connections on the distribution network was compared and analyzed. Simulations were conducted on the IEEE-33 node distribution network system to verify the effectiveness of the proposed method.

## II. PHOTOVOLTAIC, WIND TURBINE, AND BESS MODELING

### 2.1 PV model

The output power of the photovoltaics (PV) and the wind turbine (WT) is influenced by solar irradiance, temperature, wind speed, cloud cover, humidity, etc. Among these, PV is most significantly affected by solar irradiance, while WT is primarily influenced by wind speed. The solar irradiance and wind speed data involved in this paper are generated by simulation with the HOMER software. The relationship between the output power  $P_{PV}$  of PV and solar irradiance  $r$  is as follows [20]:

$$P_{PV} = \begin{cases} P_{Pe} \left( \frac{r}{r_N} \right) & 0 \leq r \leq r_N \\ P_{Pe} & r > r_N \end{cases} \quad (1)$$

where,  $P_{Pe}$  represents the rated output power of the PV;  $r_N$  is the solar irradiation amplitude when the PV output power is maximum.

### 2.2 WT model

The output power  $P_{WT}$  of the wind turbine expressed as a function of wind speed  $v$  is as follows [21]:

$$P_{WT} = \begin{cases} 0 & , 0 \leq v \leq v_{in} \text{ or } v_{out} \leq v \\ P_{WT}^{rated} \cdot \frac{v - v_{in}}{v_r - v_{in}} & , v_{in} < v \leq v_r \\ P_{WT}^{rated} & , v_r < v < v_{out} \end{cases} \quad (2)$$

where,  $v_r$  is the rated wind speed;  $v_{in}$  and  $v_{out}$  represent the cut-in wind speed and the cut-out wind speed, respectively;  $P_{WT}^{rated}$  is the rated output power of the WT.

### 2.3 BESS model

The State of Charge (SOC) of the BESS depends on the charge state at the previous moment. The SOC at each moment can be expressed as:

(1) Energy storage charging process

$$SOC(t+1) = (1 - \delta) \cdot SOC(t) + \left( \frac{\eta_c \cdot P_c(t) \cdot \Delta t}{E_{BESS}} \right) \quad (3)$$

(2) Energy storage discharge process

$$SOC(t+1) = (1 - \delta) \cdot SOC(t) - \left( \frac{P_d(t) \cdot \Delta t}{\eta_d \cdot E_{BESS}} \right) \quad (4)$$

where,  $\delta$  is the self-discharge rate;  $P_c(t)$  and  $P_d(t)$  are the charging and discharging power of BESS at moment  $t$ , respectively;  $\Delta t$  is the time interval of charging and discharging;  $E_{BESS}$  is the capacity of BESS;  $\eta_c$  and  $\eta_d$  are the charging and discharging efficiency of BESS, respectively.

### III. BI-LEVEL PLANNING MODEL FOR BESS SIZING AND SITE SELECTION

The optimization model takes into account operational optimization and economic efficiency. However, it involves a large number of variables and scales, making the planning issue complex and difficult to resolve directly. To address multi-level and large-scale optimization problems, scholars have proposed a multi-level planning framework. Its special form, bi-level planning [22], has been used extensively in electric power systems [23]-[24]. Therefore, to reduce the complexity of solving the planning problem, a bi-level optimization method to articulate the BESS planning issue was proposed in this study. In the bi-level planning, the interrelationships between the energy storage system's capacity, operational strategy, and location are considered, with the structure of the bi-level optimization model illustrated in Fig.1.

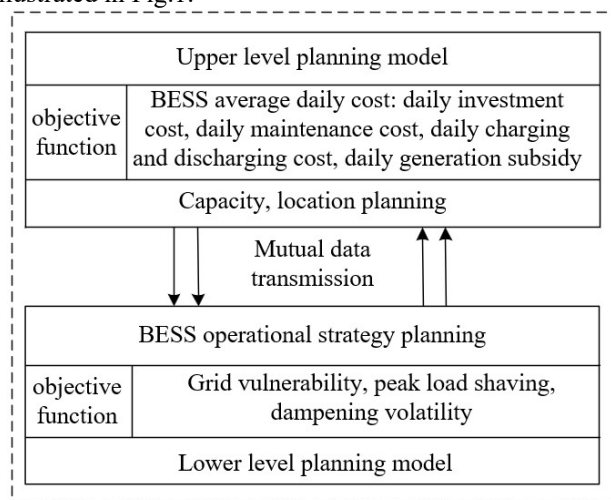


Fig. 1. Bi-level planning model structure

In a bi-level planning model, the objective function, decision variables and constraints are different for the upper and lower level model, but the optimization processes of the upper and lower layers depended on each other and required information interaction between the layers through parameter transfer: the upper level planning passed the decision variables, namely the capacity and installation location of BESS, as parameters to the lower level planning, and these parameters served as initial conditions and constraints for the optimization of lower level decision variables. Based on this, the lower level planning model performed power flow calculations and optimized the 24-hour operational strategy for BESS connected to various nodes. The objective function values obtained at the lower

level were then fed back into the objective function of the upper level, and the process iterated repeatedly until the optimum was reached.

#### 3.1 Upper level planning model

##### 3.1.1 Objective function

The minimization of average daily costs of BESS ( $C_{Total,d}$ ) as the objective function in the upper level can be formulated as:

$$C_{Total,d} = C_{I,d} + C_{OM,d} + C_{CD,d} - C_{ES,d} \quad (5)$$

where,  $C_{I,d}$ ,  $C_{OM,d}$ ,  $C_{CD,d}$  and  $C_{ES,d}$  represent the daily investment cost, daily maintenance cost, daily charging and discharging cost and daily generation subsidy of the BESS.

$$C_{I,d} = \frac{\left( \sum_{k=1}^{N_{BESS}} m \cdot E_{BESS} \right) \cdot \lambda}{365} \quad (6)$$

$$\lambda = \frac{\rho(1+\rho)^x}{(1+\rho)^x - 1} \quad (7)$$

where,  $N_{BESS}$ ,  $E_{BESS}$ ,  $m$  and  $x$  represent the number of BESS units, capacity of BESS, cost per unit capacity and investment years, respectively;  $\lambda$  is the annual capital recovery factor; and  $\rho$  is the discount rate.

$$C_{OM,d} = \frac{\left( \sum_{k=1}^{N_{BESS}} m \cdot E_{BESS} \right) \cdot 5\%}{365} \quad (8)$$

herein, the annual maintenance cost of BESS is assumed to be 5%.

$$C_{CD,d} = \sum_{k=1}^{N_{BESS}} \sum_{t=1}^{24} [\varphi_p(t) \cdot P_c(t) - \varphi_s(t) \cdot P_d(t)] \quad (9)$$

where,  $\varphi_p(t)$  and  $\varphi_s(t)$  represent the electricity purchasing and selling prices for BESS during the period time  $t$ , respectively.

$$C_{ES,d} = \sum_{k=1}^{N_{BESS}} \sum_{t=1}^{24} [0.12 \cdot P_d(t)] \quad (10)$$

where, the government subsidy for BESS is 0.12 Yuan/kWh.

##### 3.1.2 Constraints

###### (1) BESS capacity constraint

$$E_{BESS,min} \leq E_{BESS} \leq E_{BESS,max} \quad (11)$$

where,  $E_{BESS,min}$  and  $E_{BESS,max}$  are the upper and lower limits of the BESS capacity, respectively.

###### (2) SOC constraint

$$SOC_{min} \leq SOC \leq SOC_{max} \quad (12)$$

where,  $SOC_{max}$  and  $SOC_{min}$  are the upper and lower SOC limits, respectively.

###### (3) BESS energy balance constraint

$$SOC(0) = SOC(24) \quad (13)$$

To ensure the normal operation of the BESS in the next cycle, it is required that the SOC values at the beginning and end of the period are equal.

###### (4) Power balance constraint

$$P_{grid}(t) = \sum_{i=1}^{N_{bus}} P_{load,i}(t) + \sum_{l=1}^{N_l} P_{L,l}(t) - \sum_{k=1}^{N_{BESS}} P_{BESS,k}(t) - \sum_{j=1}^{N_{DG}} P_{DG,j}(t) \quad (14)$$

where,  $P_{grid}(t)$  is the absorbed/fed-in power from the upper grid,  $N_{bus}$ ,  $N_l$ ,  $N_{BESS}$ , and  $N_{DG}$  are the total number of nodes, branches, energy storage, and distributed Generations, respectively;  $P_{load,i}(t)$  is the load power of node  $i$ ;  $P_{L,l}(t)$  is

the network loss of the  $l$ th branch;  $P_{BESS,k}(t)$  is the  $k$ th BESS output power at time  $t$ ; and  $P_{DG,j}(t)$  is and the  $j$ th DG output power at time  $t$ .

(5) Node position constraints

$$\begin{cases} L_{BESS,i} \in [N_2, N_n] \\ L_{BESS,i} \neq L_{BESS,j} \end{cases} \quad (15)$$

where,  $L_{BESS,i}$  represents the node which the  $i$ th BESS is connected, the range of connected nodes is from 2 to  $n$ , and the  $i$ th BESS and the  $j$ th BESS cannot be connected to the same node.

3.2 Lower level planning model

3.2.1 Objective function

The lower level model's objective function focused on minimizing the grid's vulnerability, reducing the Peak load shaving in the system within a day, and suppressing fluctuations. It optimized the operational strategies of the BESS connected to various nodes.

(1) Grid vulnerability indicators

The vulnerability of node  $i$  at moment  $t$  is expressed as:

$$u_i(t) = \frac{\left| \frac{V_i(t)}{V_i(0)} - 1 \right|}{\Delta V_{\max}} \quad (16)$$

where,  $V_i(t)$  is the voltage of node  $i$  at moment  $t$ ;  $V_i(0)$  is the rated voltage of node  $i$ ;  $\Delta V_{\max}$  is the maximum voltage excursion.

Normalized at moment  $t$  to

$$U_i(t) = \frac{u_i(t) - u_i^{\min}(t)}{u_i^{\max}(t) - u_i^{\min}(t)} \quad (17)$$

where,  $u_i^{\max}(t)$  and  $u_i^{\min}(t)$  respectively represent the maximum and minimum values of the vulnerability of all nodes at time  $t$ .

Thus, the average value of grid vulnerability at time  $t$  is:

$$B(t) = \frac{1}{N_{bus}} \sum_{i=1}^{N_{bus}} U_i(t) \quad (18)$$

As voltage collapse at any node can potentially initiate a chain reaction of collapses at other nodes, it's imperative that the grid vulnerability index also accounts for the uniformity of vulnerability distribution across all nodes. To address this, an equilibrium index method was employed to quantify the degree of equilibrium, denoted as  $J$ , ranging from 0 to 1. Here, 0 signifies absolute equilibrium, while 1 indicates absolute disequilibrium.

The degree of equilibrium at time  $t$  is:

$$J(t) = 1 - \left[ \frac{\sum_{i=1}^N p_i(t) \log\left(\frac{1}{p_i(t)}\right)}{\log_2^N} \right]^{2//} \quad (19)$$

In the formula,  $p_i(t)$  represents the ratio of the vulnerability of node  $i$  to the total vulnerability of the grid at time  $t$ . The expression is:

$$p_i(t) = \frac{U_i(t)}{\sum_{i=1}^{N_{bus}} U_i(t)} \quad (20)$$

Finally, the average grid vulnerability indicator and the equilibrium indicator at time slice  $t$  are weighted and summed (with each weight being 0.5 in the text), and then

the average value of 24 h is calculated to obtain the final vulnerability indicator  $GV$ :

$$f_1 = GV = \frac{1}{24} \sum_{t=1}^{24} (0.5 \cdot B(t) + 0.5 \cdot J(t)) \quad (21)$$

(2) Peak load shaving

$$f_2 = P_{NL}^{\max} - P_{NL}^{\min} \quad (22)$$

where,  $P_{NL}^{\max}$  and  $P_{NL}^{\min}$  are the maximum and minimum net load power of the system for one day after connecting the BESS, respectively.

(3) Suppression of fluctuations

$$f_3 = \sum_{t=2}^{24} (P_{NL}(t) - P_{NL}(t-1))^2 \quad (23)$$

The objective function of the lower level model is described as follows:

$$\min F = k_1 f_1' + k_2 f_2' + k_3 f_3' \quad (24)$$

where,  $f_1'$ ,  $f_2'$  and  $f_3'$  are normalized to the objective functions  $f_1, f_2$  and  $f_3$  respectively;  $k_1, k_2$  and  $k_3$  are the weight coefficients of  $f_1'$ ,  $f_2'$  and  $f_3'$  respectively, satisfying  $k_1+k_2+k_3=1$ .

3.2.2 Constraints

(1) Power flow constraint

$$\begin{cases} P_j = V_j \sum_{i=1}^{N_{bus}} V_i (G_{ij} \cos \theta_{ij} + B_{ij} \sin \theta_{ij}) \\ Q_j = V_j \sum_{i=1}^{N_{bus}} V_i (G_{ij} \sin \theta_{ij} - B_{ij} \cos \theta_{ij}) \end{cases} \quad (25)$$

where,  $P_j$  and  $Q_j$  are the active and reactive power injections at node  $j$  respectively;  $V_j$  and  $V_i$  are the voltage amplitudes at node  $j$  and  $i$  respectively;  $\theta_{ij}$  is the voltage phase angle difference between node  $i$  and  $j$ ;  $G_{ij}$  and  $B_{ij}$  are the branch conductance and conductance between node  $i$  and  $j$ .

(2) Nodal voltage constraints

$$V_i^{\min} \leq V_i \leq V_i^{\max} \quad (26)$$

where,  $V_i, V_i^{\max}$  and  $V_i^{\min}$  are the voltage amplitude of node  $i$  and its upper and lower limits respectively.

#### IV. DETERMINATION OF TARGET WEIGHTING FACTORS

AHP [25] is a way to decompose a complex problem into several parts and then compare them two by two to evaluate the problem. The method quantitatively corrects the evaluation process through a nine-level scale method, the core of which is to determine the evaluation indexes and form an evaluation system. Therefore, an important step in the hierarchical analysis method is to use the nine-level scale method to construct a judgment matrix to determine the importance of each objective, the judgment matrix  $A$  can be expressed as:

$$A = [a_{ij}]_{m \times m} = \begin{bmatrix} a_{11} & a_{12} & \dots & a_{1m} \\ a_{21} & a_{22} & \dots & a_{2m} \\ \vdots & \vdots & a_{ij} & \vdots \\ a_{m1} & \dots & \dots & a_{mm} \end{bmatrix} \quad (27)$$

where,  $a_{ij}$  is the importance of the  $i$ th indicator  $f_i$  compared to the  $j$ th indicator  $f_j$ , and its value is shown in Table 2.

TABLE II  
AHP SCALE VALUES

Value of $a_{ij}$	Hidden meaning
1	$f_i$ is as important as $f_j$
3	$f_i$ is slightly more important than $f_j$
5	$f_i$ is significantly more important than $f_j$
7	$f_i$ is intensely more important than $f_j$
9	$f_i$ is extremely important compared to $f_j$
2, 4, 6, 8	Indicates the intermediate value of the above judgment
Inverse number	Importance of indicator $j$ to indicator $i$ , $m_{ji}=1/m_{ij}$

After constructing the judgment matrix, the consistency test must be carried out, which is to avoid that the indicator  $x$  is more important than the indicator  $y$ , but the final result shows that the indicator  $y$  is more important than the indicator  $x$ . If the test passes, the normalized eigenvectors are the weight coefficients of the objective function. Otherwise, the judgment matrix must be reconstructed until the consistency test passes, the specific steps are as follows.

The eigenvector  $\omega_k$ , ( $k=1, 2, 3, \dots, n$ ) corresponding to the largest eigenvalue  $\lambda_{\max}$  of the judgment matrix  $A$  is calculated, which is normalized to the weight value  $k_k$  of each indicator, denoted as:

$$k_k = \frac{\omega_k}{\sum_{k=1}^n \omega_k} \quad (28)$$

The weights corresponding to each indicator are then:

$$K = [k_1, k_2, \dots, k_n] \quad (29)$$

The consistency test is calculated as:

$$\begin{cases} C_I = \frac{\lambda_{\max} - n}{n - 1} \\ C_R = \frac{C_I}{R_I} \end{cases} \quad (30)$$

where,  $C_I$  and  $R_I$  are the consistency and random consistency indicator, respectively;  $C_R$  is the consistency ratio, whose value is less than 0.1 represents that the judgment matrix passes the consistency check;  $n$  is the number of indicators.

## V. PLANNING SOLUTION ALGORITHM

### 5.1 The original grey wolf optimizer algorithm

The grey wolf optimizer algorithm (GWO)<sup>[26]</sup> is inspired by the cooperative hunting behavior of grey wolf packs. It simulates the collaborative mechanisms observed in wolf packs to solve optimization problems. It is characterized by a stable structure and requires a few parameters to be adjusted. In GWO, grey wolves have four social ranks, in descending order of rank: alpha ( $\alpha$ ) wolves, beta ( $\beta$ ) wolves, delta ( $\delta$ ) wolves, and omega ( $\omega$ ) wolves. The first three categories of wolves guide the omega wolves in hunting prey. The mathematical model for surrounding the prey can be expressed as:

$$\vec{D} = \left| \vec{C} \cdot \vec{X}_p(t) - \vec{X}(t) \right| \quad (31)$$

$$\vec{X}(t+1) = \vec{X}_p(t) - A \cdot \vec{D} \quad (32)$$

where,  $t$  is the number of iterations;  $\vec{D}$  is the distance between the prey and the wolf;  $\vec{C}$  and  $\vec{A}$  are the coefficient

vectors;  $\vec{X}$  and  $\vec{X}_p$  are the wolf and the prey position vector, respectively. The vectors  $\vec{A}$  and  $\vec{C}$  are calculated as follows:

$$\vec{A} = 2 \cdot a \cdot r_1 - a \quad (33)$$

$$\vec{C} = 2 \cdot r_2 \quad (34)$$

where  $r_1$  and  $r_2$  are random values between [0,1]; the convergence factor  $\vec{a}$  takes values in the range [0,2] and decreases linearly as the number of iterations increases.

The mathematical model for chasing prey is detailed in reference [26].

### 5.2 Improved grey wolf optimizer

Like other intelligent algorithms, the initial population in the grey wolf optimizer is generated randomly. If the initial population generation is overly concentrated it will affect the results of the solution scheme. Additionally, the grey wolf optimizer also faces the issue of premature convergence. To address these two points, an improved grey wolf optimizer is proposed in this paper.

#### (1) Generating initial population using tent mapping

The basic GWO cannot ensure that the initial population is uniformly distributed in the solution space. Chaotic sequences have the advantages of randomness, regularity, and ergodicity. Compared to other mappings, the tent mapping generates more uniform sequences. Therefore, this paper utilizes tent mapping for the initialization of the grey wolf population. The tent mapping can be expressed as:

$$x_{t+1} = \begin{cases} \frac{x_t}{u} & 0 \leq x_t < u \\ \frac{1-x_t}{1-u} & u \leq x_t \leq 1 \end{cases} \quad (35)$$

where the distribution sequence generated is most uniform when  $u$  is taken as 0.5, and this belongs to the most typical tent mapping<sup>[27]</sup>, when the distribution density is insensitive to parameter changes. Then equation (35) can be transformed into equation (36).

$$x_{t+1} = \begin{cases} 2x_t & 0 \leq x_t < 0.5 \\ 2(1-x_t) & 0.5 \leq x_t \leq 1 \end{cases} \quad (36)$$

Based on the tent mapping, the population  $Y$  is represented as:

$$Y = Y_{\min} + x_t \cdot (Y_{\max} - Y_{\min}) \quad (37)$$

#### (2) Improved convergence factor

The convergence factor influences the search capability of the grey wolf algorithm. The original grey wolf algorithm employs a linear convergence factor, but the convergence process in most optimization problems is non-linear. Therefore, this paper introduces an exponential function to improve the convergence factor  $a$ . The new non-linear convergence factor is represented as:

$$a = 2 - \frac{2(e^{\frac{T}{T}} - 1)}{e - 1} \quad (38)$$

where,  $T$  is the maximum number of iterations.

The curve of the improved convergence factor compared to the original one is shown in Fig.2. The absolute value of slope for the improved convergence factor increases from small to large, which is beneficial for the algorithm to diverge better in the early stages of iteration, facilitating the

search for the global optimum, and later improving the convergence speed of the algorithm.

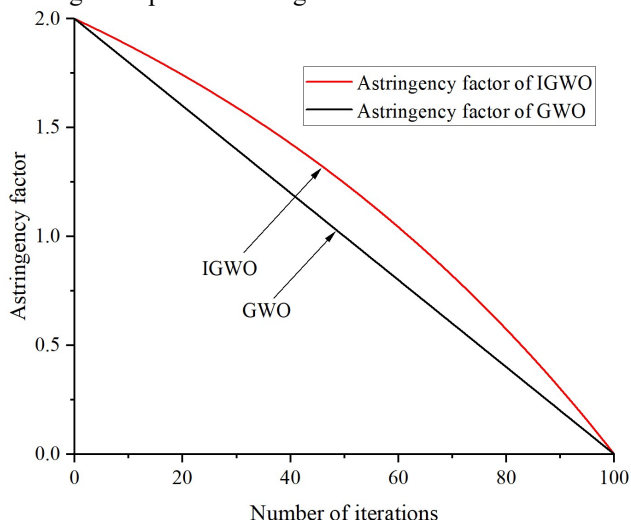


Fig. 2. Convergence factor curve before and after improvement

With the large number of variables and dimensions in the bi-level planning model and the complexity of the solution problem, this paper encodes the location of the proposed bi-level grey wolf algorithm based on the idea of interactive iteration as shown in Fig.3.

The upper level planning consisted of two parts: the capacities and the connection locations of the  $n$  BESS units, totaling  $2*n$  dimensions, as shown in Fig.3(a). The lower level planning involved the power output of each BESS unit from the first to the  $n$ th for every hour of the day, totaling  $24*n$  dimensions, as shown in Fig.3(b).

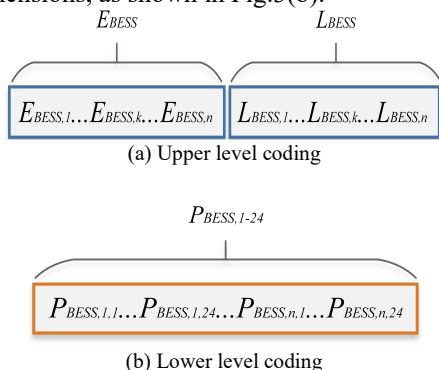


Fig. 3. Bi-level coding structure

The process of the designed bi-level algorithm is illustrated in Fig.4.

The specific steps of the proposed algorithm are as follows:

Step 1: Input the data of the distribution network to be planned and the algorithm parameters. Both the upper and lower populations are set to 30, with a maximum of 100 iterations.

Step 2: Initialize the upper level wolf pack by tent mapping and set the upper level iteration count  $i=0$ .

Step 3: Pass the initialized population of the upper level to the lower level as known quantities, initialize the lower level wolf pack by tent mapping, and set the lower level iteration count  $j=0$ .

Step 4: Input the BESS capacity and connection locations passed from the upper level, along with the BESS output obtained from the lower level initialization, into the system

for power flow calculation, obtaining the lower level fitness function values.

Step 5: Increase the lower level iteration count by one:  $j=j+1$ , and update the positions of the lower level wolf packs. If  $j < j_{max}$ , return to Step 3; otherwise, input the lower level results obtained in Step 4 back into the upper level fitness function.

Step 6: Calculate the value of the upper level fitness function, update the position of the upper level wolf packs, and increment the upper level iteration count by one,  $i=i+1$ .

Step 7: Check if the upper level iteration count meets  $i < i_{max}$ . If it does, return to Step 2; otherwise, output the bi-level optimization configuration results of BESS.

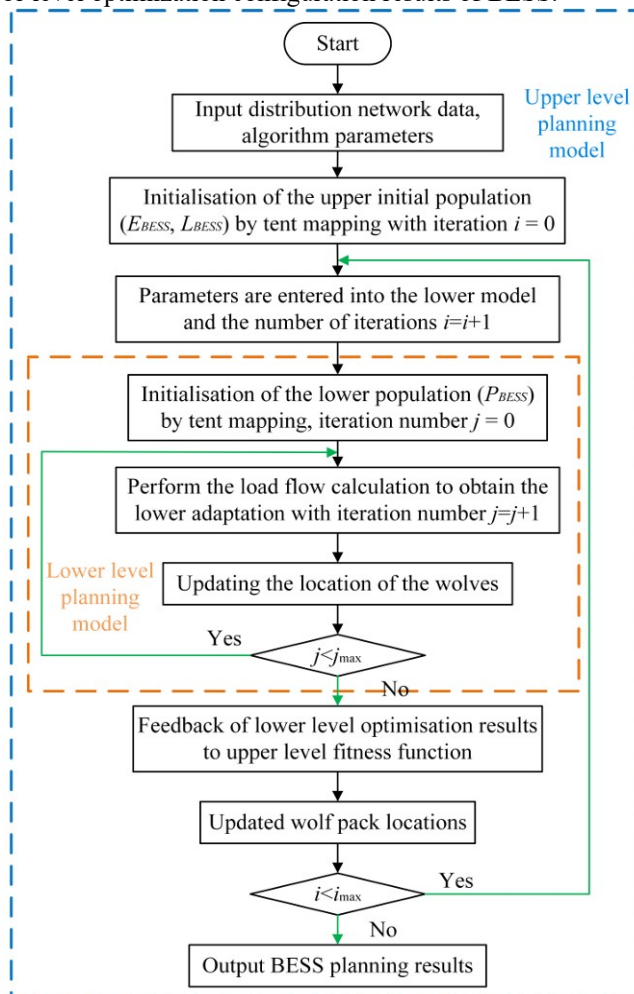


Fig. 4. Flow of the bi-level planning algorithm

## VI. SIMULATION ANALYSIS FOR THE PROPOSED BI-LEVEL MODEL

### 6.1 Parameter settings

To validate the performance of the proposed bi-level planning model, a simulation analysis was conducted using the modified IEEE 33-node distribution system, as illustrated in Fig.5. The voltage amplitude is 12.66 kV, with a total load of 3715 kW + 2300 kvar. System parameters can be found in reference [28]. A 400 kW photovoltaic system was allocated at node 28, and 300 kW wind turbines were connected at nodes 9, 20, and 25. The typical daily load curve is depicted in Fig.6, while the typical daily output of PV and WT, calculated using equations (1) and (2), is presented in Fig.7.

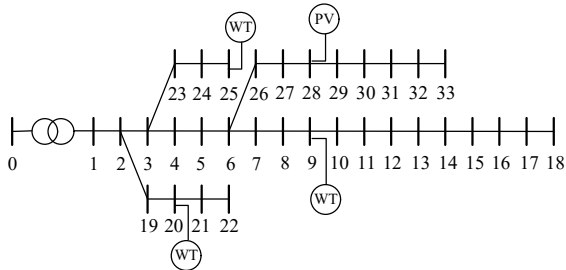


Fig. 5. Modified IEEE33-node system

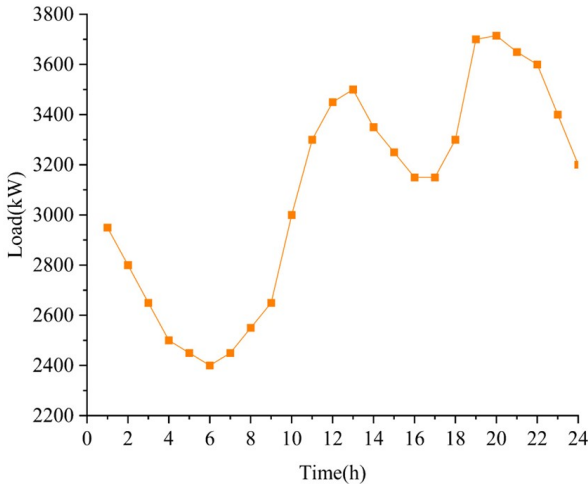


Fig. 6. Typical daily load characteristic curve

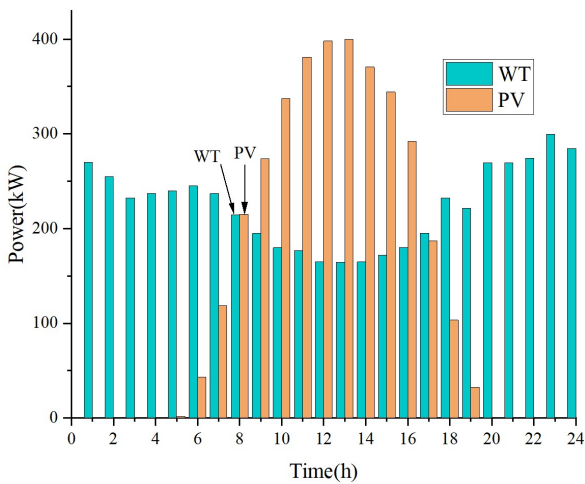


Fig. 7. Typical daily output of PV and WT

In this paper, it is considered that among the three indicators, peak shaving is the most important, followed by grid vulnerability and suppressing load fluctuations is the least important. Upon comparison, peak shaving is slightly more important than grid vulnerability; grid vulnerability is slightly more important than suppressing load fluctuations. The judgment matrix obtained in section 3 is as follows:

$$A = \begin{bmatrix} 1 & 1/2 & 2 \\ 2 & 1 & 3 \\ 1/2 & 1/3 & 1 \end{bmatrix} \quad (39)$$

As calculated by equation (30), the judgment matrix yielded a consistency ratio  $C_R$  of  $0.088 < 0.1$ , indicating that it passed the consistency test. The weight values for each objective function are  $[0.297, 0.5396, 0.1634]$ , i.e.,  $k_1=0.297$ ,  $k_2=0.5396$ ,  $k_3=0.1634$ .

6.2 Case study

In order to verify the effectiveness of the bi-level planning

models and algorithms proposed in this paper, a comparative analysis is carried out through the following four scenarios.

Scenario 1: BESS is not accessed;

Scenario 2: BESS for single access, SOC range is set to 40%-60%, 25%-75%, 10%-90% respectively, and optimized using GWO algorithm.

Scenario 3: 2-4 nodes are selected to access BESS, respectively, with the appropriate SOC range obtained based on Scenario 2, and the GWO algorithm is used for optimization.

Scenario 4: Based on the results of Scenario 3, the optimal number of BESS accesses is determined and analyzed using the IGWO and PSO algorithms for comparison.

The results of the optimal allocation of BESS under the different scenarios are shown in Table 5. A positive average daily cost of BESS indicates daily expenditure, while a negative cost indicates profitability for the scenario.

The parameters of BESS and time-of-use electricity price are presented in Tables 3 and 4, respectively.

TABLE III  
PARAMETERS OF THE BESS

Parameters	Values
Unit capacity cost ( $10^3$ Yuan/MWh)	127
Year of investment/(year)	10
Discount rate/%	6.332
Charging/discharging efficiency	0.95
SOC initial value	0.5
Self-discharge rate/%	0.1

TABLE IV  
TIME-OF-USE ELECTRICITY PRICE

Time(h)	Price (Yuan/kWh)
00:00-07:00 23:00-24:00	0.3818
07:00-10:00 15:00-18:00	0.8395
10:00-15:00 18:00-21:00	1.3222

Table 5 illustrates that without BESS integration, the grid vulnerability index is 0.4610, the load peak-to-valley difference is 0.3721 p.u., and the load fluctuation value is 0.051. Upon integrating BESS, there was a notable reduction in both grid vulnerability and load peak-to-valley difference, accompanied by an enhancement in load fluctuation suppression. All these indicators showed improvement. Additionally, in each scenario, BESS units were strategically located near branching nodes, terminal nodes, and distributed energy sources within the distribution network, effectively contributing to power support.

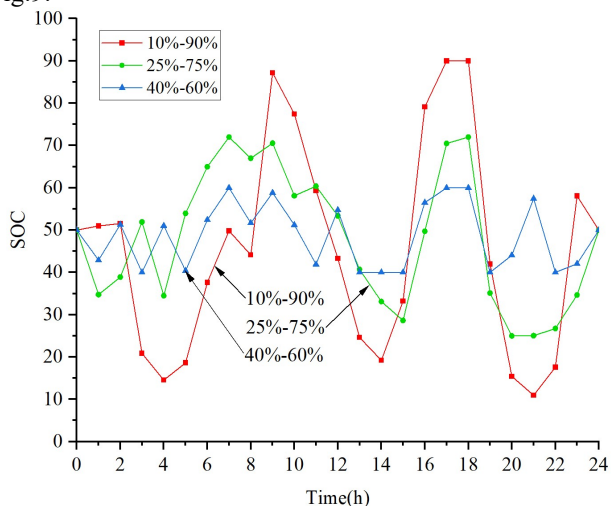
In Scenario 2, the BESS with the SOC range from 10% to 90% demonstrated superior voltage regulation, maximum power adjustment capacity, and optimal performance in load fluctuation suppression. As the SOC allowable range increased, the average daily cost of BESS decreased from 153.7 Yuan to 67.104 Yuan. Meanwhile, the grid vulnerability index decreased, the peak load shaving and load fluctuation further reduced. In order to reflect more clearly the impact of different SOC allowable ranges on planning, the BESS output and the SOC curve under Scenario 2 are presented in Fig.8, respectively.

Combined with Table 5 and Fig.8, it is evident that when the SOC range is 40%-60%, the BESS is connected to node 32 with an access capacity of 0.3835 MWh, in this case, there is irregular charging and discharging behavior of the

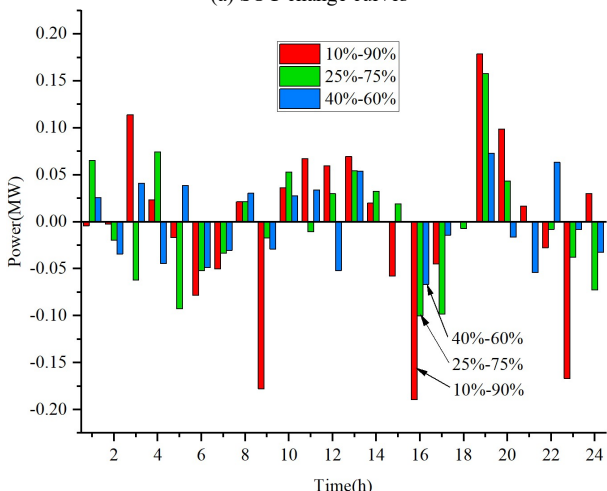
TABLE V  
RESULTS OF THE OPTIMAL CONFIGURATION OF BESS UNDER DIFFERENT SCENARIOS

Scenarios	The number of BESS	Solution algorithm	SOC range	BESS planning results		Upper level objective function	Lower level objective function		
				Nodes/ capacity (MWh)	Average daily cost (Yuan)	Grid vulnerability	Peak load shaving (p.u.)	Load fluctuation	
Scenario 1	/	/	/	/	/	/	0.4610	0.3721	0.0511
Scenario 2	1	GWO	40%-60%	32 / 0.3835	153.70	0.4606	0.3443	0.0431	
			25%-75%	17 / 0.4501	18.642	0.4591	0.3252	0.0402	
			10%-90%	17 / 0.3917	-67.104	0.4572	0.3107	0.0378	
Scenario 3	2	GWO	10%-90%	17 / 0.7799	32 / 0.4593	-242.23	0.4426	0.2530	0.0261
				3 / 0.4836	17 / 0.4022	10.972	0.4479	0.2746	0.0292
				32 / 0.4344					
Scenario 4	2	PSO	10%-90%	16 / 0.6309	17 / 0.6407	-149.88	0.4459	0.2576	0.0304
		IGWO		16 / 0.4904	17 / 1.0582	-410.80	0.4408	0.2510	0.0234

BESS. This phenomenon can be attributed to the limited SOC allowable range, which hinders the optimal functioning of the BESS. It becomes apparent that with a wider SOC available range, BESS units exhibit the ability to discharge during peak load periods and charge during low load periods. The power curves of net load in Scenario 2 are shown in Fig.9.



(a) SOC change curves



(b) Power of BESS

Fig. 8. Variation of BESS output and SOC for each BESS in Scenario 2

In Fig.9, the red line depicts the net load curve with a SOC range of 10%-90%. Compared to the net load curves under the other two SOC ranges, the peaks and valleys of the net

load curve under the SOC available range of 10%-90% are significantly reduced, measuring 0.7603 p.u. and 0.4496 p.u., respectively. At this point, the peak-to-valley difference is 0.3107 p.u., which is 16.50% lower than the pre-optimization period.

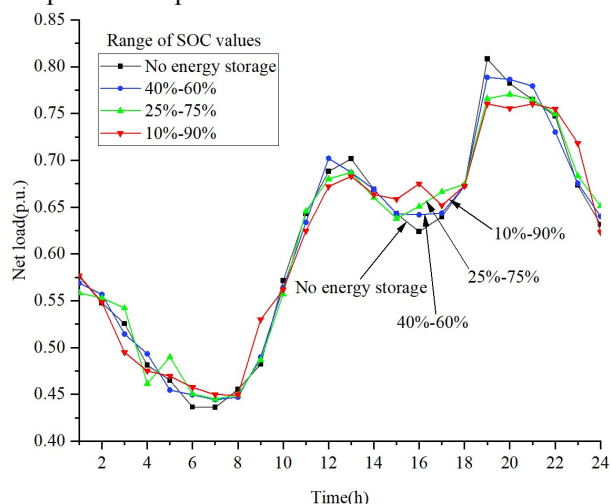


Fig. 9. Net load curves in Scenario 2

This verifies that a larger available range of SOC is preferred, and considering the life of the storage and maintaining its energy level to prevent overcharging and over-discharging, the BESS with a SOC range of 10%-90% is selected for subsequent work.

The BESS with SOC ranging from 10% to 90% is selected in Scenario 3, and from two to four BESSs are connected sequentially in the distribution network for comparative analysis. The SOC as well as the operation strategy of BESSs at different nodes are shown in Fig.10.

Combined with Fig.10 and Table 5, it can be seen that on the whole no matter how many BESSs are connected to the distribution network, they can cooperate, discharging during peak hours, charging during low valley hours, and adjusting the technical parameters during the rest of the day in accordance with the constraints of the individual objective functions.

From Table 5, it is observed that as the number of BESSs increases from one to four, the average daily costs of BESS, peak load shaving, and load fluctuation initially decrease and then increase. Each objective function has an optimal value at the access of two BESSs. Compared to no BESS,

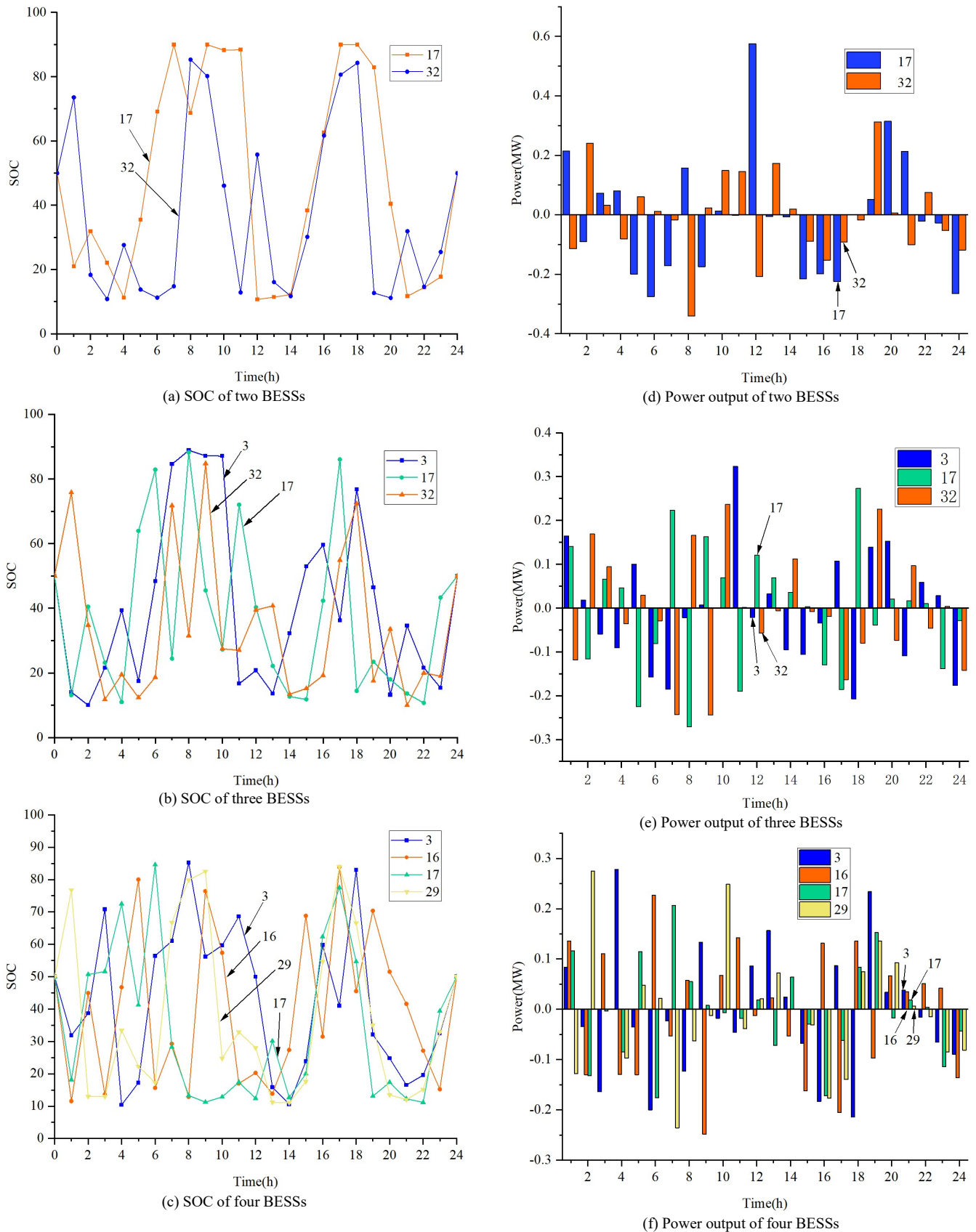


Fig. 10. The SOC and power output of BESSs in Scenario 3

the average daily cost of BESS is -242.23 Yuan which obtained the optimal economy, the grid vulnerability index is 0.4426, a reduction of 3.99%, and the load fluctuation index is 0.0261 with a reduction of 48.92%. However, connecting more than two BESSs to the distribution network leads to an increase in grid vulnerability, as well as worsened peak load shaving and load fluctuation.

The results of BESS accessing two points in the distribution network are better than the results of accessing one point, which can be summarized for the following reasons: Firstly, an extra BESS can dispatch more power to gain profit through time-sharing tariff arbitrage. What is more, there has been a decrease in the average daily cost of the BESS. Secondly, the extra BESS can also take part in the

peak shifting task of the distribution network, which leads to an improvement of the peak-to-valley difference and a reduction of load fluctuation.

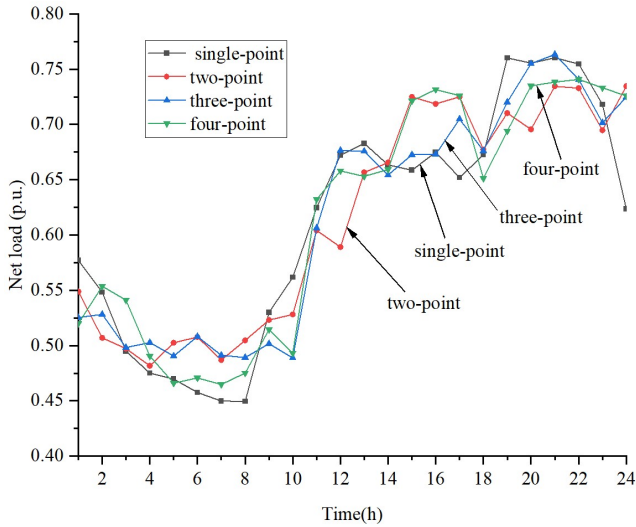


Fig. 11. Net load curves in Scenario 3

In Scenario 4, the proposed IGWO algorithm is employed to determine the optimal configuration of the two BESS units integrated into the distribution network. The SOC, operation strategy and net load profile of the BESSs are shown in Fig.12, Fig.13, and Fig.14, respectively.

As Table 5 shows, the average daily cost of BESS after optimization using the IGWO algorithm in scenario 4 is -410.8 Yuan, which is more profitable than that of the GWO algorithm by 168.57 Yuan per day, and the grid vulnerability indicator, peak load shaving and load fluctuation are 0.4408, 0.2510p.u. and 0.0234 respectively, which are 4.06%, 0.79% and 10.34% less than that optimized by GWO algorithm, and 4.38%, 32.55% and 54.21% less than the scenario without BESS respectively. In contrast, the average daily cost of BESS, grid vulnerability index, peak load shaving, and load fluctuation after optimization using the PSO algorithm are -149.88 Yuan, 0.4459, 0.2576, and 0.0304, respectively. These results are inferior to those optimized by the GWO and IGWO algorithms, indicating that the PSO algorithm is less effective than the GWO algorithm in handling high-dimensional, nonlinear, and complex problems.

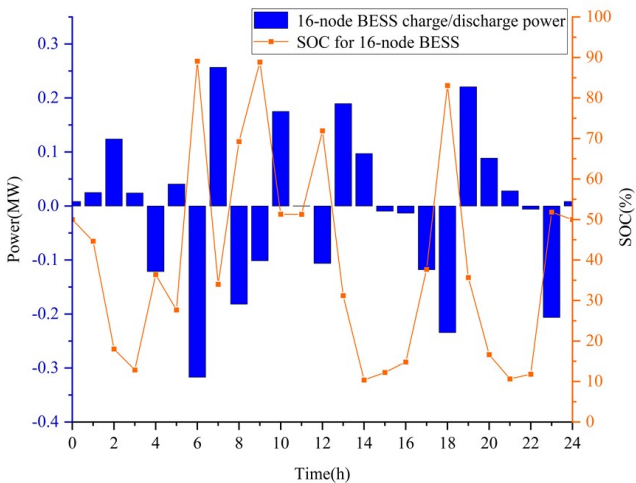


Fig. 12. The operation strategy and SOC curve of the 16-node BESS

From Fig.12, Fig.13 and Fig.14, it can be seen that the

overall trend of operation strategies is both discharging at peak loads and charging at valley loads in Scenario 4. Additionally, the BESS engages in charging and discharging activities during the remaining periods to facilitate arbitrage while maintaining equilibrium with various distribution network indicators. Taking the BESS at node 17 as an example, the BESS discharges power to the distribution grid in conjunction with the WT from 0:00 to 4:00, effectively lowering the net load curve during this period. Subsequently, from 5:00 to 9:00, the BESS absorbs surplus power, thereby elevating the load trough. Following this, from 9:00 to 14:00, coinciding with peak electricity prices, the BESS discharges power to the distribution grid in coordination with the PV. This action not only mitigates the initial peak of the load curve but also enables tariff arbitrage. Between 15:00 and 17:00, the BESS is recharged at reduced tariffs. Furthermore, from 18:00 to 21:00, in conjunction with ample wind resources and higher tariffs, the BESS supplies power to the distribution network. This not only reduces the second peak of the load curve but also leverages tariff differentials for profit.

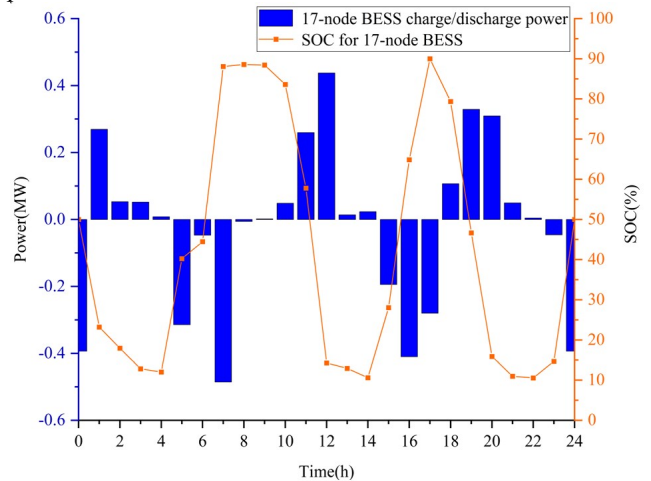


Fig. 13. The operation strategy and SOC curve of the 17-node BESS

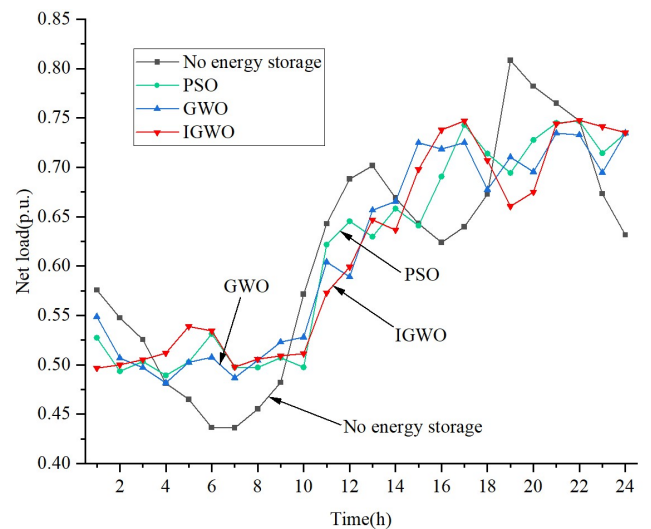


Fig. 14. Net load curves in Scenario 4

Throughout the day, the SOC values of the two BESS units consistently remain within the range of 10% to 90%. Specifically, at 0:00 and 24:00, both BESS units are at a SOC value of 50%. This practice serves to prevent overcharging and over-discharging of the BESS units, thereby enhancing their service life. Moreover, maintaining

the SOC within this range ensures an adequate energy reserve to optimize various distribution network indicators for the following day.

From Fig.14, it can be seen that the net load curve optimized by the IGWO algorithm is smoother compared to the GWO algorithm, which verifies the superiority of the IGWO algorithm proposed in this paper.

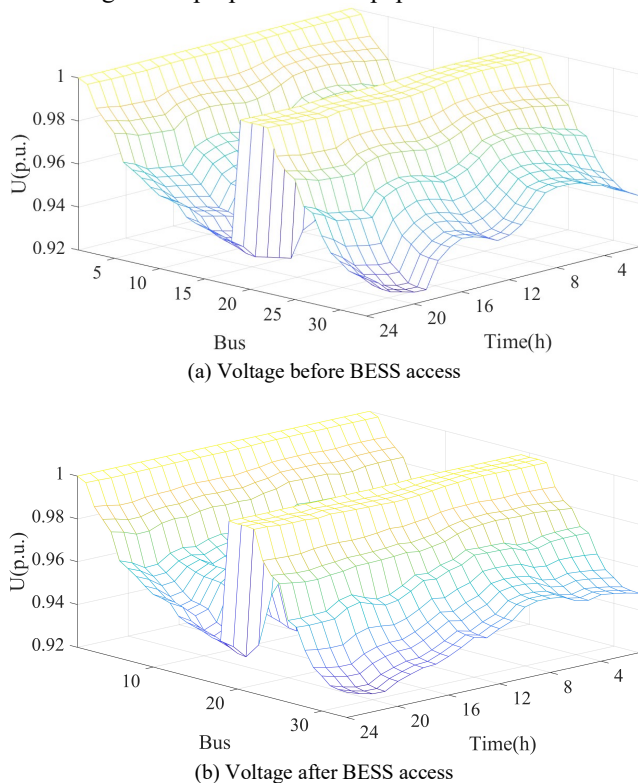


Fig. 15. Voltage before and after BESS access

Fig.15(a) shows the voltage profile before installing the BESS, and Fig.15(b) shows the node voltage profile at Scenario 4. In one day, the voltage magnitude is as low as 0.9253 p.u. without BESS access and 0.9271 p.u. after BESS access. Furthermore, voltage curves become smoother.

### VII. CONCLUSION

In this study, we comprehensively assessed the economic, safety, and reliability aspects of the distribution network for establishing a bi-level optimization configuration model of BESS units. By orchestrating the optimization processes at both upper and lower levels, the potential of BESS in the distribution network was fully exploited. Under the verification of the IEEE 33-node distribution network system, the conclusions are as follows:

(1) The IGWO algorithm is developed by incorporating tent chaotic mapping and a nonlinear convergence factor to enhance the performance of the GWO algorithm. This augmentation renders the IGWO algorithm notably more effective in tackling high-dimensional and nonlinear challenges, such as optimizing BESS.

(2) The AHP method is utilized to transform the lower level complex multi-objective optimization problem into a multi-level single-objective problem. This transformation simplifies the computational process and facilitates clear and concise results.

(3) Various SOC ranges of BESS are individually optimized, revealing that larger SOC ranges enhance both the economic efficiency of BESS and its regulatory impact on distribution network indices. However, to mitigate the risks of overcharging and over-discharging, SOC operation is typically confined within the range of 10% to 90%. This constraint not only safeguards the service life of BESS but also ensures its sustained operational reliability.

(4) After connecting varying numbers of BESS units to the distribution network, it is determined that optimal outcomes are achieved when two BESS units are integrated. Utilizing the IGWO algorithm facilitates the attainment of optimal economic efficiency, and after BESS integration, the grid's vulnerability index, peak-to-valley difference, and load fluctuation decreased by 4.38%, 32.55%, and 54.21%, respectively, compared to the case without BESS.

### REFERENCES

- [1] L. Hou, H. J. Lin, X. Yang, T. K. Yang, F. Qu, and D. Shao, "Optimal Scheduling of Integrated Energy Systems for High-speed Railway Stations Considering Integrated Demand Response under the Carbon Market," *IAENG International Journal of Applied Mathematics*, vol. 53, no.2, pp 497-506, 2023.
- [2] Yi Zhang, Lin Li, and Wei Hu, "An Integrated Energy Demand Response Model Considering Source-Load Synergy and Stepped Carbon Trading Mechanism," *Engineering Letters*, vol. 32, no. 3, pp 614-624, 2024.
- [3] Jie Qian, Yuhang Peng, Haoling Zheng, and Xi Wang, "Application of Improved Seagull Optimization Algorithm on Optimal Allocation Optimizations of Distributed Generation," *Engineering Letters*, vol. 31, no.3, pp 1151-1159, 2023.
- [4] P. Kumar, N. K. Swamkar, A. Ali, O. P. Mahela, and B. Khan, "Transmission network loss reduction and voltage profile improvement using network restructuring and optimal DG placement," *Sustainability*, vol. 15, no. 2, pp 976, 2023.
- [5] Gonggui Chen, Jiajie Li, Yuansen Xu, Bo Peng, Hao Tan, and Hongyu Long, "Optimal Configuration of Renewable Energy DGs Based on Improved Northern Goshawk Optimization Algorithm Considering Load and Generation Uncertainties," *Engineering Letters*, vol. 31, no.2, pp 511-530, 2023.
- [6] Liang Zhang, Liang Chen, Wenwei Zhu, Ling Lyu, Guowei Cai, Koh Leong Hai, "Research on the optimal allocation method of source and storage capacity of integrated energy system considering integrated demand response," *Energy Reports*, Vol. 8, pp 10434-10448, 2022.
- [7] Yang B, Wang J T, Chen Y X, et al. "Optimal sizing and placement of energy storage system in power grids: a state-of-the-art one-stop handbook," *Journal of Energy Storage*, vol. 32, 101814, 2020.
- [8] Fatemeh Mohammadi Behbahani, Bahman Ahmadi, Ramazan Caglar, "Multi-objective multiverse optimization for optimal allocation of distributed energy resources: The optimal parallel processing schemes," *Electric Power Systems Research*, vol. 231, 110298, 2024.
- [9] Choton K. Das, Octavian Bass, Thair S. Mahmoud, Ganesh Kothapalli, Mohammad A.S. Masoum, Navid Mousavi, "An optimal allocation and sizing strategy of distributed energy storage systems to improve performance of distribution networks," *Journal of Energy Storage*, 100847, 2019.
- [10] Xiao, H., Yi, X., Ding, S. and Su, S, "Optimal configuration method based on optimal expected power characteristics for micro power supply and energy storage device," *IET Renewable Power Generation*, vol. 12, pp 1876-1882, 2018.
- [11] Dawei Su, Zhen Lei, "Optimal configuration of battery energy storage system in primary frequency regulation," *Energy Reports*, pp 157-162, 2021.
- [12] Luo Y, Tian P, Yan X, Xiao X, Ci S, Zhou Q, Yang Y, "Energy Storage Dynamic Configuration of Active Distribution Networks—Joint Planning of Grid Structures," *Processes*, vol. 12, no. 1, pp 79, 2024.
- [13] Xu W, Yu B, Song Q, Weng L, Luo M, Zhang F. Economic and Low-Carbon-Oriented Distribution Network Planning Considering the Uncertainties of Photovoltaic Generation and Load Demand to Achieve Their Reliability. *Energies*. vol. 15, no. 24, 2022.
- [14] Yang Li, Bo Feng, Bin Wang, Shuchao Sun, "Joint planning of distributed generations and energy storage in active distribution

- networks: A Bi-Level programming approach, "Energy, vol. 245, 2022.
- [15] Zhang J, Zhu L, Zhao S, Yan J, Lv L, "Optimal Configuration of Energy Storage Systems in High PV Penetrating Distribution Network," *Energies*, vol. 16, no. 5, 2023.
- [16] Wei, Y, Zhao, B, Hu, J. et al. "A Two-Layer Planning Method for Distributed Energy Storage with Multi-point Layout in High Photovoltaic Penetration Distribution Network," *Journal Of Electrical Engineering & Technology*, 2024.
- [17] Siyu Zhou, Yang Han, Shuheng Chen, Ping Yang, Karar Mahmoud, Mohamed M.F. Darwish, Lehtonen Matti, Amr S. Zalhaf, "A multiple uncertainty-based Bi-level expansion planning paradigm for distribution networks complying with energy storage system functionalities," *Energy*, vol. 275, 127511, 2023.
- [18] Hossein Saber, Moein Moeini-Aghtaie, Mehdi Ehsan, "Developing a multi-objective framework for expansion planning studies of distributed energy storage systems (DESSs)," *Energy*, vol. 157, pp 1079-1089, 2018.
- [19] S. Mahapatra et al., "Implementation of PSO, its variants and Hybrid GWO-PSO for improving Reactive Power Planning, 2019 Global Conference for Advancement in Technology (GCAT)," pp 1-6, 2019.
- [20] Evangelopoulos V.A, Georgilakis P.S. "Optimal distributed generation placement under uncertainties based on point estimate method embedded genetic algorithm," *IET Generation Transmission & Distribution*, vol. 8, no. 3 pp 389-400, 2014.
- [21] Li Zhi, Ye Lin, Zhao Yonging, et al. "short-term wind power prediction based on extreme learning machine with error correction," *Protection and Control of Modern Power Systems*, vol. 1, no. 1, pp 40-47, 2016.
- [22] Nantian Huang, Xuanyuan Zhao, Yu Guo, Guowei Cai, Rijun Wang, "Distribution network expansion planning considering a distributed hydrogen-thermal storage system based on photovoltaic development of the Whole County of China, " *Energy*, vol. 278, 2023.
- [23] B. Huang, T. Zhao, M. Yue and J. Wang, "Bi-Level Adaptive Storage Expansion Strategy for Microgrids Using Deep Reinforcement Learning," *IEEE Transactions on Smart Grid*, vol. 15, no. 2, pp 1362-1375, 2024.
- [24] Y. Bian, P. Lu, L. Xie, J. Ye, L. Ma and J. Yang, "Bi-level optimal configuration of hybrid shared energy storage capacity in wind farms considering prediction error," *CSEE Journal of Power and Energy Systems*
- [25] Yunxiao Zhang, Xinyu Zhao, Yu Zhao, Xin Cui, Yongchang Zhang, Haisen Zhao, "Pre-selection scheme evaluation of hybrid energy storage for distribution network based on utility combination method," *Journal of Energy Storage*, vol. 88, 111497, 2024.
- [26] Faisal Al Thobiani, Samir Khatir, Brahim Benaissa, Emad Ghandourah, Seyedali Mirjalili, Magd Abdel Wahab, "A hybrid PSO and Grey Wolf Optimization algorithm for static and dynamic crack identification," *Theoretical and Applied Fracture Mechanics*, vol. 118, 103213, 2022.
- [27] Yutong Li, Yu Liu, Chunli Lin, Jiayao Wen, Pengguo Yan, and Yukun Wang, "An Improved Pelican Optimization Algorithm Based on Chaos Mapping Factor," *Engineering Letters*, vol. 31, no.4, pp1605-1634, 2023.
- [28] Wang H, Wang J, Piao Z, et al. "The Optimal Allocation and Operation of an Energy Storage System with High Penetration Grid-Connected Photovoltaic Systems," *Sustainability*, vol. 12, no. 15, pp 6154, 2020.